Proceedings of the ASME 2010 3rd Joint US-European Fluids Engineering Summer Meeting and 8th International Conference on Nanochannels, Microchannels, and Minichannels
FEDSM-ICNMM2010
August 1-5, 2010, Montreal, Canada

FEDSM-ICNMM2010-30369

A METHOD TO QUANTIFY MIXING IN A TWO COMPONENT FLUIDIZED BED

Norman K. Keller and Theodore J. Heindel*
Department of Mechanical Engineering
Iowa State University
Ames, Iowa 50011

ABSTRACT

Fluidized bed technology can be used for pyrolysis and gasification of solid fuel particles such as biomass, which is important to industry because of its potential as an alternative for petroleum-based fuels. To efficiently utilize a fluidized bed reactor it is necessary, among other factors, to investigate the mixing and segregation behavior of the fuel particles with the bed material. In order to characterize the material distribution, a technique to visualize the biomass inside a fluidized bed reactor has been developed using X-ray computed tomography (CT) scans. This paper presents an image analysis procedure that can be used to quantify and characterize the local mixing and segregation in a 3D fluidized bed.

Keywords: biomass processing, fluidized bed, hydrodynamics, mixing, segregation, X-ray computed tomography

INTRODUCTION

With expected shortages in fossil fuel supplies and due to legislation efforts promoting 'green' energy, renewable energies such as biomass, converted to different forms of fuels, have gained a lot of interest in the past decade. Studies on the potential of biomass to serve as a sustainable and economical energy source have addressed many important aspects that must be considered [1-7]. According to these studies, the most promising technology to convert biomass into useful forms of fuels is thermochemical processing, utilizing a fluidized bed reactor for either pyrolysis or gasification. The advantages of a fluidized bed reactor are its high heat and mass transfer rates, low pressure drop and efficient mixing properties. Although many studies have been carried out on the characteristics of fluidized beds, with significant contributions as early as the 1970s [8-16], mixing and segregation are still poorly understood. The opaque nature of a fluidized bed reactor prohibits direct visual observations; therefore many findings of early studies have been either based on 2D reactors or carried out by means of invasive measurement techniques [17, 18].

This paper describes the use of 3D X-ray computed tomography scans of a laboratory scale fluidized bed reactor to study mixing and segregation in a two component bed of granular material. The bed is composed of glass beads (GB) representing inert bed material and ground walnut shell (GWS) as model biomass. The procedures outlined here will be used in future studies that address mixing and segregation in a fluidized bed.

EXPERIMENTAL SETUP

Fluidized bed reactor

As illustrated in Figure 1, the cold-flow fluidized bed used in this study is composed of a 10.2 cm inner diameter acrylic tube, and includes a plenum, bed chamber, and riser or free-board region. The distributor, mounted between the plenum and bed chamber, is made of an acrylic plate containing 63 1 mm diameter holes drilled in concentric circles, giving the aeration plate an open area ratio of 0.62%. To prevent particles from falling through the holes or plugging them, a fine mesh screen is placed right above the distributor plate. Air enters the plenum through the inlet in the bottom of the plenum, which is filled with marbles to evenly disperse the air over the bottom of the aeration plate. The model reactor features various other taps for pressure transducers and side injection. Since these have not been used in this study, they have been plugged. Additionally, the method developed and described below was tested in a static bed, so no air flow was recorded. Future work will apply the analysis method in a fluidized bed.

* Corresponding Author: T.J. Heindel, theindel@iastate.edu

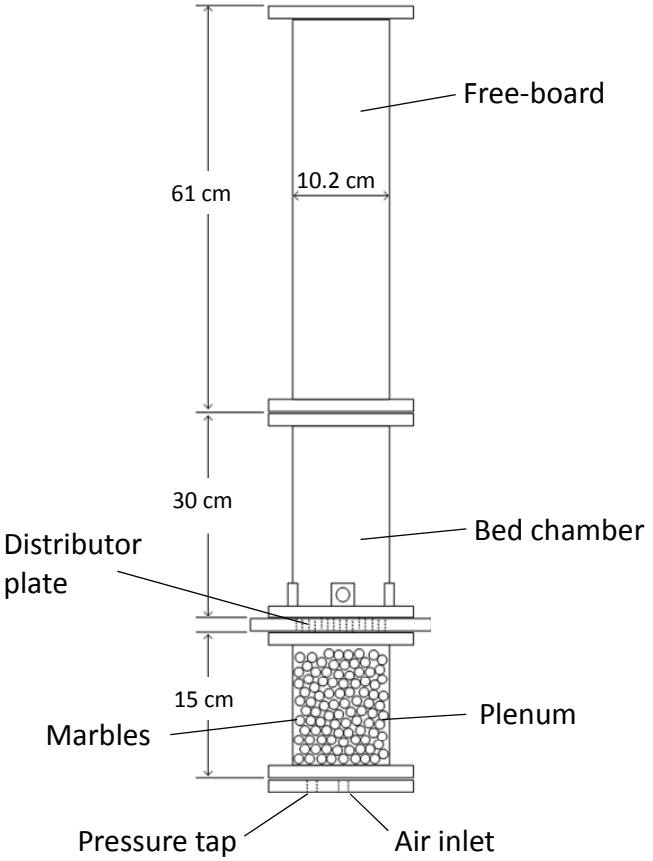

FIGURE 1: SCHEMATIC OF MODEL FLUIDIZED BED REACTOR.

Material selection

The materials selected for this study are based on what is used in large scale industrial fluidized beds. The inert bed material is represented by glass beads in the 500-600 µm range. The second component, modeling the biomass, is ground walnut shell also in the 500-600 µm range. The properties of the particles used in this study are summarized in Table 1.

TABLE 1: PROPERTIES OF BED MATERIALS.

Particle properties	Glass beads	Ground walnut shell
diameter [µm]	500-600	500-600
particle density [g/cm^3]	2.6	1.2-1.4

The properties of glass beads are very similar to those of refractory sand, which is usually used in industrial reactors, but glass beads are better characterized and uniform. Figure 2a shows a high resolution photograph of the particles in the 500-600 µm size range. Most glass bead particles are spherical, smooth and solid.

The second component in the fluidized bed, which simulates the biomass, is ground walnut shell, also in the 500-600 µm size range. Figure 2b shows a high resolution photograph of the ground walnut shell particles. Note that the particles do not appear to be spherical although they are often modeled as such.

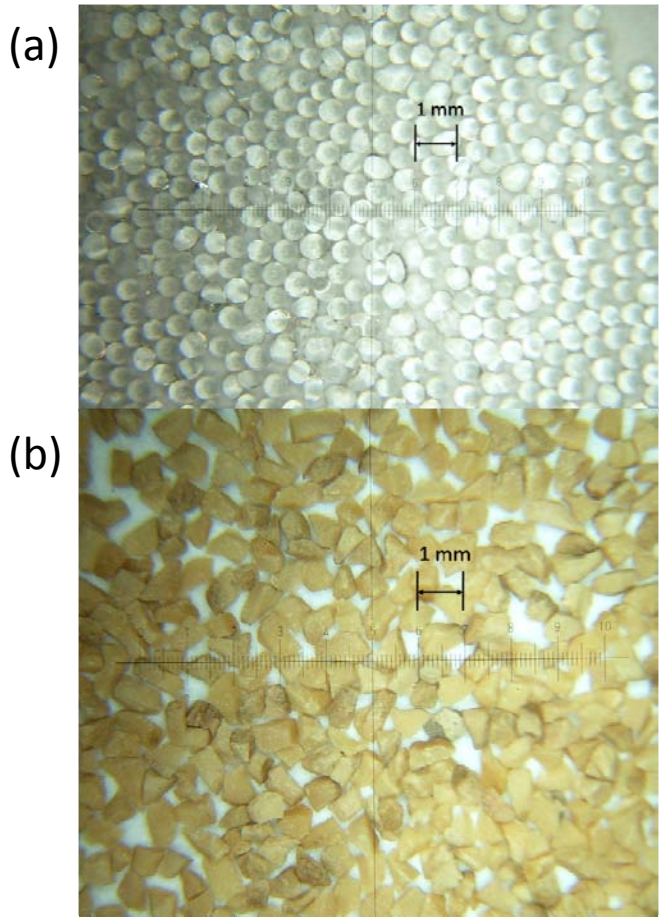

FIGURE 2: CLOSE-UP PHOTOGRAPHS OF PARTICLES USED IN THIS STUDY: (a) 500-600 µm GLASS BEADS AND (b) 500-600 µm GROUND WALNUT SHELL.

X-ray imaging facility

The X-ray imaging facility at Iowa State University is a unique, non-invasive measurement tool specifically developed for opaque, multiphase flows. Since it has been described elsewhere [19-22] only a brief description is given here.

As Figure 3 illustrates, two LORAD LPX200 X-ray sources are mounted perpendicular to each other on a 1m inner diameter gear ring that can rotate 360°. The sources allow for variable voltage (10–200 kV) and current (0.1–10 mA) up to a total power output of 900 W for each source. Low energy radiation is suppressed by a combination of 1 mm thick copper and aluminum filters. Mounted opposite of the X-ray sources are two image intensifier/CCD camera pairs. This system setup is capable of acquiring radiographs, stereographs and computed tomography scans.

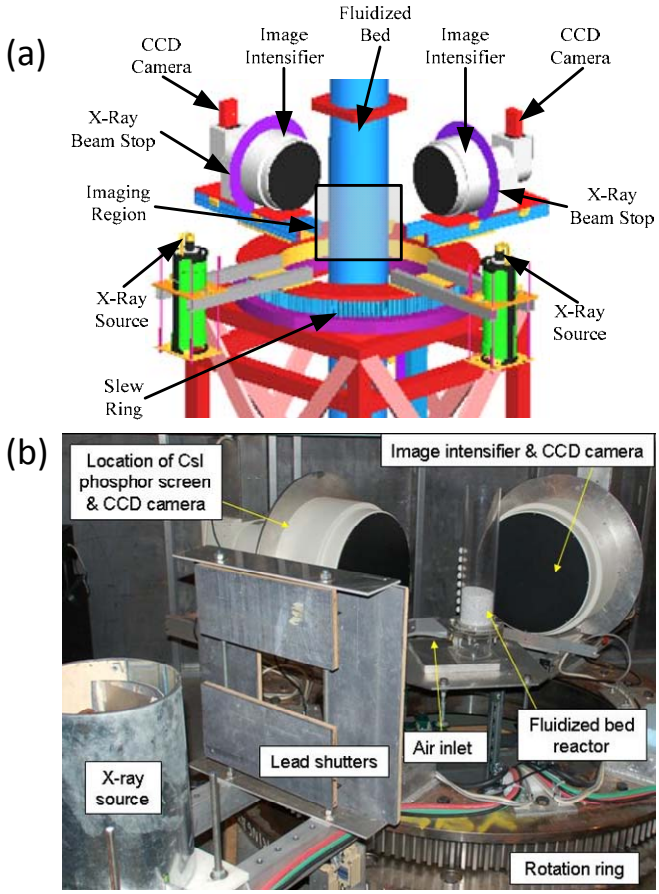

FIGURE 3: X-RAY IMAGING FACILITY; (a) SCHEMATIC AND (b) PICTURE.

For improved computed tomography scans, a 44×44 cm cesium-iodide scintillator screen is used in this study as the detector and transforms radiation into visible light. The image is captured by an Apogee Alta U9 system with a 50 mm Nikon lens. This system has 3072×2048 pixels and is thermoelectrically cooled to allow for long exposure times.

Computed tomography scans

To acquire X-ray CT data, the scanner rotates around the object of interest, taking a series of 2D projections at different angles which are later back-projected using a reconstruction algorithm and custom computer programs [19-21, 23, 24]. This procedure yields a digital 3D image for further analysis. The local variation of voxel intensity, where a voxel is a 3D pixel, in this 3D array corresponds to the attenuation variation of the X-ray beam as it passes through the object, which in turn is a function of density, material thickness and attenuation coefficient, this is later used to derive the material distribution inside the reactor.

The reconstructed 3D images of the object can be filtered (i.e., sliced) to show internal structure of the mixture as shown in Figure 4. Because the voxels hold intensity data, the slice images are in gray scale; however, images can be given a false color to improve contrast. All images reported in this study will only show x-slices. The reported CT values are averaged over concentric annuli or averaged over horizontal slices.

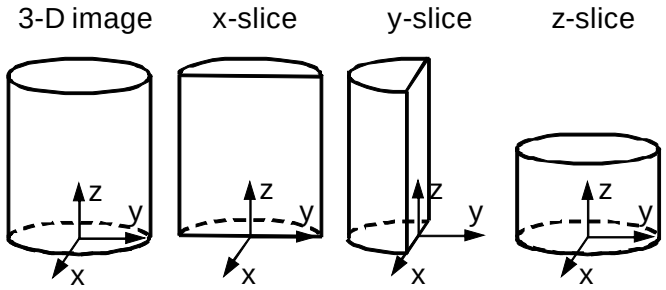

FIGURE 4: CT IMAGING PLANES.

Beam hardening

The most commonly encountered artifact in X-ray CT imaging is beam hardening. It is caused by lower energy X-rays being more readily attenuated than higher energy X-rays. It is therefore a function of material density, material thickness, and attenuation coefficient. It causes the edges to appear lighter and the center to appear darker in the reconstructed image. Hence, for a cylindrical object of uniform density, the CT value would vary with radius. Figure 5 shows the effects of beam hardening for a full bed of glass beads (top curve) and a full bed of ground walnut shell (bottom curve). The higher density glass beads are more affected by beam hardening, while the lower density ground walnut shell show almost no effect at all. The values are the average for concentric annuli with one pixel wall thickness. The effects of beam hardening complicates the analysis when determining mixing and segregation between glass beads and ground walnut shell.

Usually, beam hardening can be accounted for by applying a correction algorithm for known material density. However, since this study deals with mixing and segregation of two components inside the bed, the density of any control volume will vary with time and location. Therefore, a primary objective of the analysis and development method has been to properly account for beam hardening.

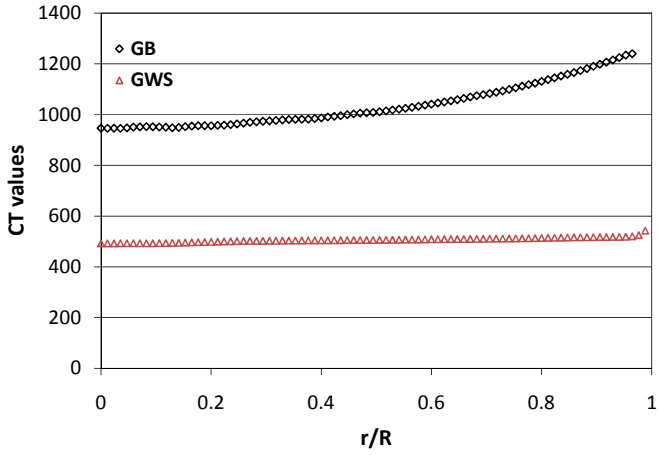

FIGURE 5: AVERAGE CT VALUES FOR CONCENTRIC ANNULI IN THE BED.

RESULTS AND DISCUSSION

For this study all experiments have been conducted with a static fluidized bed. The X-ray source settings were 150 keV and 3.5 mA. The X-ray beam was filtered with one aluminum filter and one copper filter. Images were acquired for every degree, totaling 360 images, with the camera set at 4×4 binning. The system was configured to yield a voxel size of roughly 580 µm on a side. Figure 6 provides an illustration where the left side shows the x-slice or center plane of the bed material and the right side is a magnified voxel.

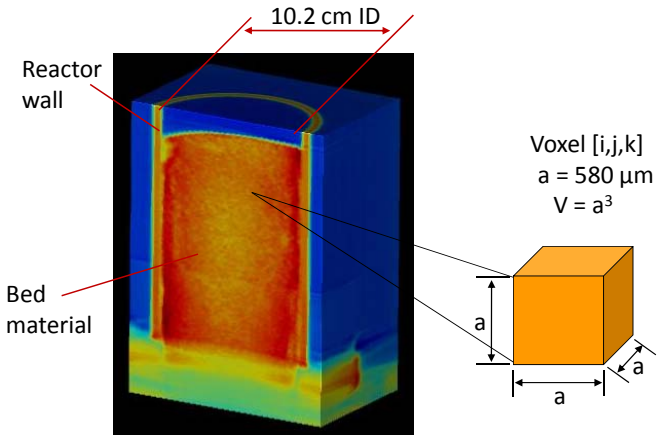

FIGURE 6: 3D CT IMAGE OF A BED OF GRANULAR MATERIAL CUT THROUGH THE CENTER (X-SLICE).

To calibrate voxel intensity to mixing composition, a series of CT scans were performed with different composition ratios of well-mixed systems. Eleven different bed compositions were scanned, ranging from pure glass beads to pure ground walnut shell, with a uniformly incremented volume ratio. Table 2 summarizes these experimental conditions.

TABLE 2: OVERVIEW OF CALIBRATION EXPERIMENTS.

Experiment	Volume ratio
1	100% GB
2	10% GWS + 90% GB, well-mixed
3	20% GWS + 80% GB, well-mixed
4	30% GWS + 70% GB, well-mixed
5	40% GWS + 60% GB, well-mixed
6	50% GWS + 50% GB, well-mixed
7	60% GWS + 40% GB, well-mixed
8	70% GWS + 30% GB, well-mixed
9	80% GWS + 20% GB, well-mixed
10	90% GWS + 10% GB, well-mixed
11	100% GWS

As shown in Figure 5, the CT values are a function of bed radius, whereas Figure 7 shows the CT values, which are averaged horizontally, are not a function of bed height. The error bars in Figure 7 represent one standard deviation from the averaged values. In general, the average CT value is uniform through the entire bed height. The small variations in the 25% GWS - 75% GB system are attributed to small nonuniformities in the local mixing.

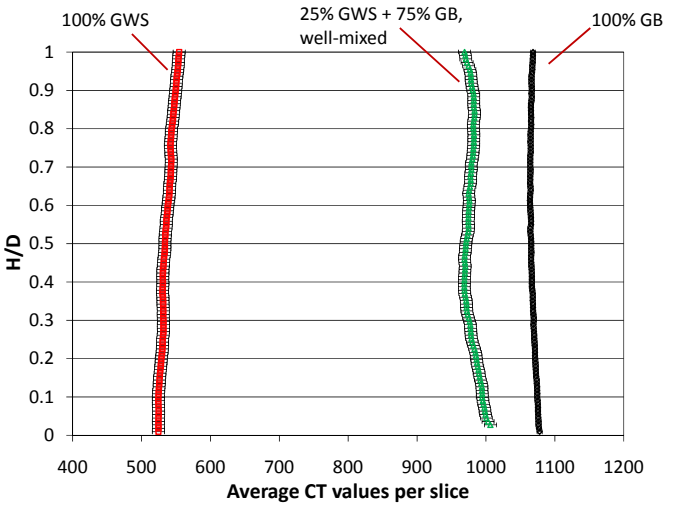

FIGURE 7: VARIATION OF AVERAGE CT VALUES OVER BED HEIGHT WITH STANDARD DEVIATION.

Assuming a homogeneous particle distribution, CT values were averaged over concentric radii and plotted as a function of radius. These data were used to generate a matrix that correlates the voxel values to the biomass volume fraction as a function of the distance to the center (radius) of the bed. The values in the matrix are the average CT values calculated for concentric annuli. This calibration is possible because the variation over the bed height is minimal (Figure 7) and beam hardening uniformly affects the values within the annulus.

Figure 8 shows a summary of the acquired data for the composition calibration. The curves are the CT values averaged for concentric annuli for mixture ratios in 10% steps by volume. The nonlinearity of the respective curves result from beam hardening. The top curve represents a bed of pure GB, showing the largest impact of beam hardening due to the high density of the material. This causes higher CT values towards the edge of the bed and lower CT values in the center. The almost flat curve on the bottom represents a bed of pure GWS, which has negligible beam hardening. The curves in between are for the different volume ratios between GB and GWS. Note that image saturation near the wall, where the X-ray path length through the bed is a minimum, results in increased noise in the data; these data are not shown in Figure 8.

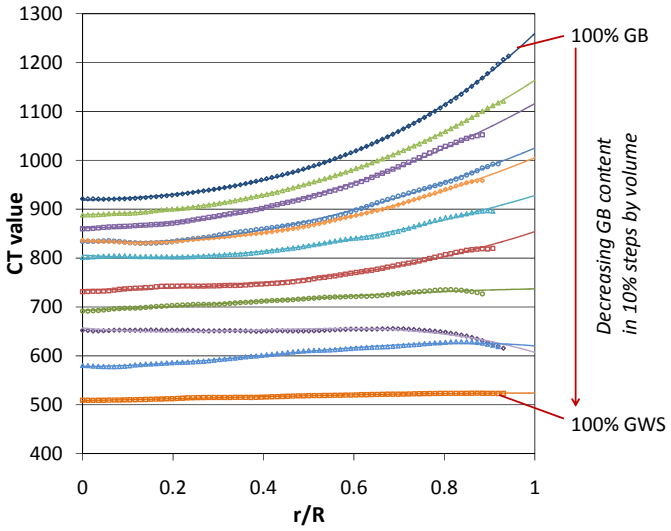

FIGURE 8: CT VALUES AS FUNCTION OF RADIUS AND MIXTURE RATIO.

Third order polynomial curve-fits have been generated from each curve in Figure 8 and summarized in Table 3. The curves have been extrapolated all the way to the bed wall. These curve-fits were used to generate a bed composition matrix for the respective CT value as a function of bed radius. The composition matrix is then used as a "look-up table" for the local voxel CT value at a particular radius to determine the voxel biomass composition on a volume basis. Hence, the 3D data are transformed from local CT value to local biomass composition within the entire 3D volume.

TABLE 3: POLYNOMIAL CURVE FIT CORRELATIONS FROM THE CURVES IN FIGURE 8.

Experiment	Curve fit correlation
1	$y = 218x^3 + 91.2x^2 + 31.7x + 918$
2	$y = 63.1x^3 + 200x^2 + 11.6x + 889$
3	$y = 2.82x^3 + 249x^2 + 2.43x + 862$
4	$y = -49.6x^3 + 289x^2 - 49.6x + 835$
5	$y = -16.5x^3 + 238x^2 - 51.1x + 835$
6	$y = -30.3x^3 + 212x^2 - 59.9x + 806$
7	$y = 80.2x^3 + 23.8x^2 + 15.6x + 734$
8	$y = -34.4x^3 + 41.4x^2 + 37.4x + 693$
9	$y = -216x^3 + 277x^2 - 130x + 707$
10	$y = -154x^3 + 192x^2 + 3.93x + 578$
11	$y = -16.2x^3 + 15.7x^2 + 15.4x + 509$

Concept validation

The procedures outlined above have been validated using a mixture of known composition of glass beads and ground walnut shell. In this way, the total volume of biomass present in a random mixture of known composition is compared to the initial biomass volume. To verify that independently acquired data can be analyzed with this concept, a series of experiments with two component static beds, varying in composition and material distribution, have been carried out and analyzed. Example results are summarized in Table 4. The variation listed with the initial volume was determined by estimating the potential height variation of ± 1-2 mm. With a 10.2 cm diameter bed, a variation of biomass volume is expected to be on the order of ± 16 cm^3. The absolute error reported is associated with the calculated volume of biomass.

TABLE 4: VALIDATION OF CONCEPT.

Bed composition	Condition	Initial volume [cm^3]	Calculated vol [cm^3]	Absolute Error [%]
25% GWS + 75% GB	I	208 ± 16	248	19.6
	II	208 ± 16	211	1.67
50% GWS + 50% GB	I	415 ± 16	416	0.37
	II	415 ± 16	409	1.46
75% GWS + 25% GB	I	623 ± 16	664	6.62
	II	623 ± 16	636	2.29

As shown in Table 4, the majority of the calculated biomass volume in the random mixtures are well within the initial volume. A significant source of potential error is the flange region at the base of the bed, which affects the X-ray absorption in this region. For example, Figure 9 shows sample results for 50% GWS and 50% GB. The reconstructed 3D image sliced through the center is shown on the top with added false-color. The reconstructed x-slice is shown on the bottom left and the transformed data is shown on the bottom right with white representing 100% biomass and black indicating 100% glass beads, and the gray-scale indicating the local variation between the two. The flange region identified by the red oval causes false biomass identification because of the thicker flange region. This causes a false identification of biomass in this region. Depending on the amount of model biomass within the region of the flange, the associated error can be significant. For this reason, the flange region was omitted from the analysis summarized in Table 4. We are currently modifying the bed chamber such that the aeration plate is above the flange region to eliminate this error.

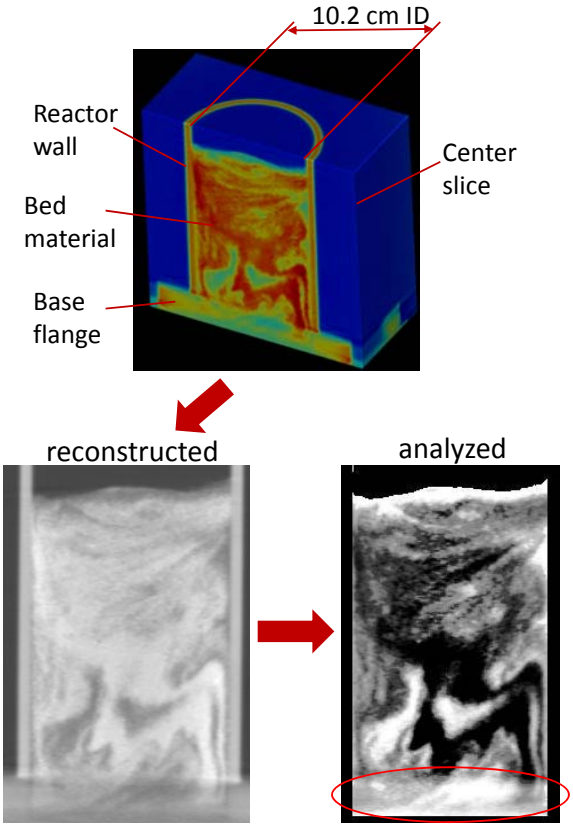

FIGURE 9: SAMPLE BIOMASS IDENTIFICATION USING 50% GWS AND 50% GB.

An additional source of error is in the generation of the transformation matrix. A homogenous mixture was assumed, but local variations, if they exist, can produce false calibration values.

Figures 10-12 represent x-slices from the various mixtures identified in Table 4. Mix I and mix II identify two different random mixtures of the same composition. The analyzed region omitted the flange region. In general, the procedures outlined above identify the mixture biomass regions, and from this identification, provide a good estimate of the known biomass content (i.e., Table 4). The most significant error (i.e., 25% GWS + 75% GB, mix I) occurs when the biomass remains outside the flange region (see mix I in Figure 10) resulting in an overestimation of biomass in the entire mixture. This is the primary reason for the large error identified in Table 4 for mix I of the 25% GWS and 75% GB mixture. The calculated biomass volume improves when it appears a uniform amount of biomass is in the flange region. The modified aeration plate identified above will improve the analysis procedures by eliminating the flange from the region of interest.

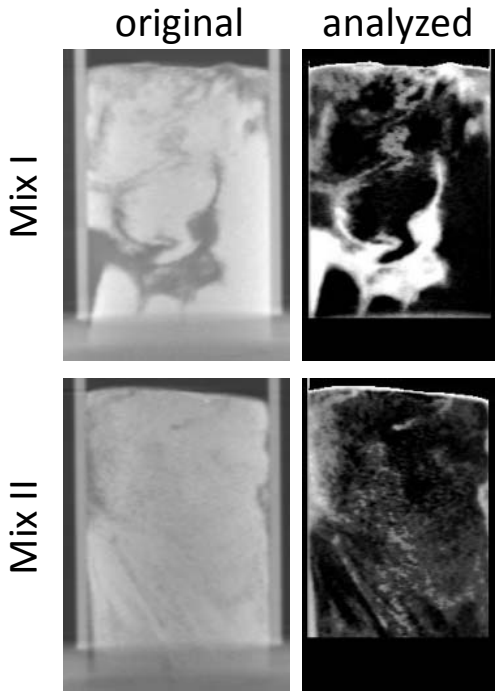

FIGURE 10: CENTER SLICE OF ORIGINAL CT SCAN AND ANALYZED FILE FOR A 25% GWS AND 75% GB BED, MIX I AND II REFER TO TABLE 4.

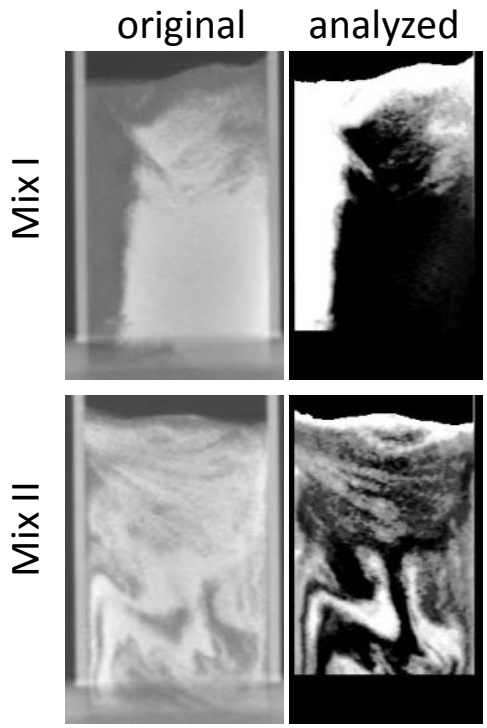

FIGURE 11: CENTER SLICE OF ORIGINAL CT SCAN AND ANALYZED FILE FOR A 50% GWS AND 50% GB BED, MIX I AND II REFER TO TABLE 4.

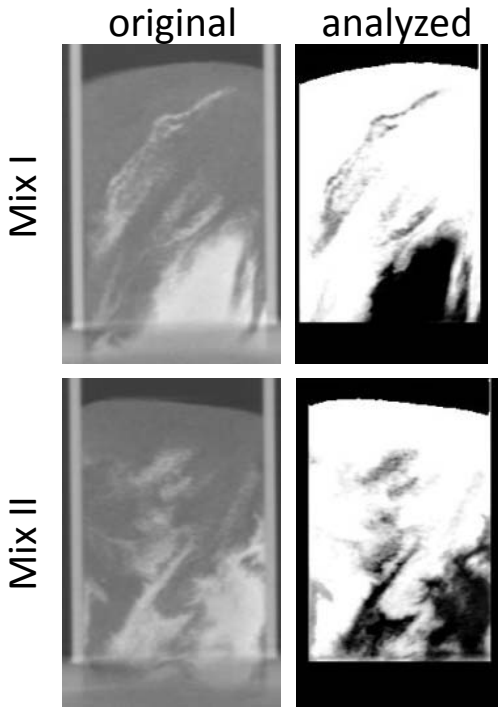

FIGURE 12: CENTER SLICE OF ORIGINAL CT SCAN AND ANALYZED FILE FOR A 75% GWS AND 25% GB BED, MIX I AND II REFER TO TABLE 4.

CONCLUSIONS

A process using X-ray computed tomography has been outlined to systematically quantify mixing and segregation in a two component fluidized bed. It has been shown that by this process, spatial analysis of a fluidized bed is possible. Although only one system is considered in this paper, GWS and GB, investigation in other systems is ongoing.

It is important to note that although it has been shown that the principal method is feasible, errors associated with bed geometry must be addressed. Specifically, a modified bed aeration plate is proposed to eliminate the flange from the region of interest.

Future work will address mixing and segregation in an operating fluidized bed that undergoes sudden collapse to "freeze" the particle distribution.

ACKNOWLEDGMENTS

Support for portions of the work described in this paper from ConocoPhillips Company is acknowledged.

REFERENCES

[1] Balat, M., "Biomass Energy and Biochemical Conversion Processing for Fuels and Chemicals", *Energy Sources, Part A: Recovery, Utilization, and Environmental Effects*, 28: 517 - 525 (2006).

[2] Balat, M., Acici, N. and Ersoy, G., "Trends in the Use of Biomass as an Energy Source", *Energy Sources, Part B: Economics, Planning, and Policy*, 1: 367 - 378 (2006).

[3] Brown, R. C., "Biorenewable Resources", Iowa State Press (2003).

[4] Demirbas, A., "Biomass Resource Facilities and Biomass Conversion Processing for Fuels and Chemicals", *Energy Conversion and Management*, 42: 1357-1378 (2001).

[5] Kaygusuz, K., "Hydropower and Biomass as Renewable Energy Sources in Turkey", *Energy Sources, Part A: Recovery, Utilization, and Environmental Effects*, 23: 775 - 799 (2001).

[6] Kelly-Yong, T. L., Lee, K. T., Mohamed, A. R. and Bhatia, S., "Potential of Hydrogen from Oil Palm Biomass as a Source of Renewable Energy Worldwide", *Energy Policy*, 35: 5692-5701 (2007).

[7] Searcy, E., Flynn, P., Ghafoori, E. and Kumar, A., "The Relative Cost of Biomass Energy Transport", *Applied Biochemistry and Biotechnology*, (2007).

[8] Hoffmann, A. C., Janssen, L. P. B. M. and Prins, J., "Particle Segregation in Fluidised Binary Mixtures", *Chemical Engineering Science*, 48: 1583-1592 (1993).

[9] Nienow, A. W., Rowe, P. N. and Chiba, T., "Mixing and Segregation of a Small Proportion of Large Particles in Gas Fluidized Beds of Considerably Smaller Ones", *AIChE Symp Ser*, 74: 45-53 (1978).

[10] Rice, R. W. and Brainovich, J. F. J., "Mixing/Segregation in Two- and Three-Dimensional Fluidized Beds: Binary

Systems of Equidensity Spherical Particles", *AIChE Journal*, 32: 7-16 (1986).
[11] Rowe, P. N. and Nienow, A. W., "Minimum Fluidisation Velocity of Multi-Component Particle Mixtures", *Chemical Engineering Science*, 30: 1365-1369 (1975).
[12] Rowe, P. N. and Nienow, A. W., "Particle Mixing and Segregation in Gas Fluidised Beds. A Review", *Powder Technology*, 15: 141 - 147 (1976).
[13] Rowe, P. N. and Yacono, C. X. R., "The Bubbling Behaviour of Fine Powders When Fluidised", *Chemical Engineering Science*, 31: 1179-1192 (1976).
[14] Wirsum, M., Fett, F., Iwanowa, N. and Lukjanow, G., "Particle Mixing in Bubbling Fluidized Beds of Binary Particle Systems", *Powder Technology*, 120: 63-69 (2001).
[15] Zhang, Y., Jin, B. and Zhong, W., "Fluidization, Mixing and Segregation of a Biomass-Sand Mixture in a Fluidized Bed", *International Journal of Chemical Reactor Engineering*, 6: (2008).
[16] Zhang, Y., Jin, B. and Zhong, W., "Experimental Investigation on Mixing and Segregation Behavior of Biomass Particle in Fluidized Bed", *Chemical Engineering and Processing: Process Intensification*, 48: 745-754 (2009).
[17] Goldschmidt, M. J. V., Link, J. M., Mellema, S. and Kuipers, J. A. M., "Digital Image Analysis Measurements of Bed Expansion and Segregation Dynamics in Dense Gas-Fluidised Beds", *Powder Technology*, 138: 135-159 (2003).
[18] Zhang, Y., Jin, B., Zhong, W., Ren, B. and Xiao, R., "Characterization of Fluidization and Segregation of Biomass Particles by Combining Image Processing and Pressure Fluctuations Analysis", *International Journal of Chemical Reactor Engineering*, 7: (2009).
[19] Ford, J. J., Heindel, T. J. and Jensen, T. C., "Imaging a Gas-Sparged Stirred-Tank Reactor with X-Ray Ct", *2007 Proceedings of the 5th Joint ASME/JSME Fluids Engineering Summer Conference*, 1: 445-452 (2007).
[20] Heindel, T. J., Gray, J. N. and Jensen, T. C., "An X-Ray System for Visualizing Fluid Flows", *Flow Measurement and Instrumentation*, 19: 67-78 (2008).
[21] Heindel, T. J., Hubers, J. L., Jensen, T. C., Gray, J. N. and Striegel, A. C., "Using X-Rays for Multiphase Flow Visualization", *2005 ASME Fluids Engineering Division Summer Meeting*, 2005: 2095-2103 (2005).
[22] Hubers, J. L., Striegel, A. C., Heindel, T. J., Gray, J. N. and Jensen, T. C., "X-Ray Computed Tomography in Large Bubble Columns", *Chemical Engineering Science*, 60: 6124-6133 (2005).
[23] Franka, N. P., "Visualizing Fluidized Beds with X-Rays", *Mechanical Engineering*, M.S. Thesis: (2008).
[24] Franka, N. P., Heindel, T. J. and Battaglia, F., "Visualizing Cold-Flow Fluidized Beds with X-Rays", *Proceedings of the 2007 ASME International Mechanical Engineering Congress and Exposition*, (2007).